Efficient Deep Learning for Massive MIMO Channel State Estimation

Mason del Rosario

Doctoral Exit Seminar

September 2022

Outline

Background

Feedback-based estimation of channel state information in MIMO networks.

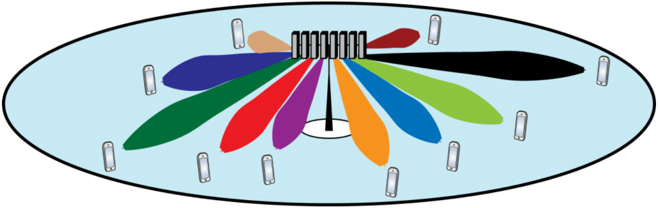

MIMO and CSI

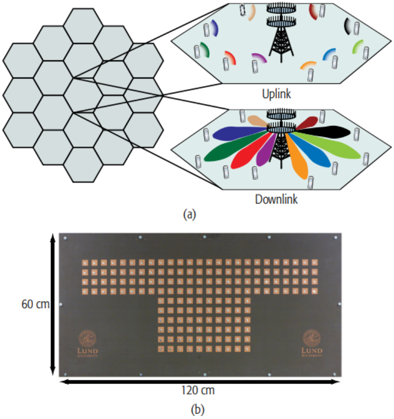

- MIMO = Multiple input multiple output

E. Björnson, E. G. Larsson, and T. L. Marzetta, "Massive MIMO: Ten Myths and One Critical Question," *IEEE Communications Magazine*, vol. 54, no. 2, pp. 114–123, 2016

MIMO and CSI

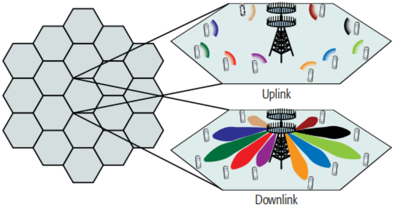

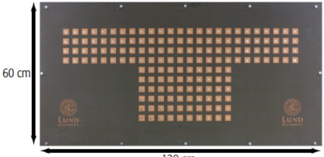

- MIMO = Multiple input multiple output
- Massive w.r.t. antenna count, not physical size.

E. Björnson, E. G. Larsson, and T. L. Marzetta, "Massive MIMO: Ten Myths and One Critical Question," *IEEE Communications Magazine*, vol. 54, no. 2, pp. 114–123, 2016

MIMO and CSI

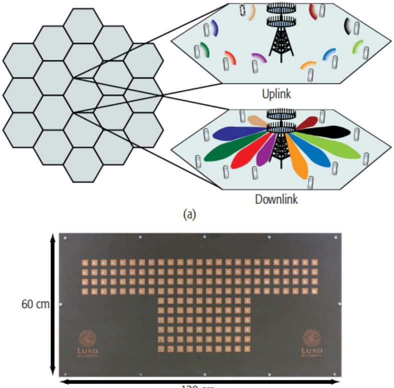

(a)

(b)

- MIMO = Multiple input multiple output
- Massive w.r.t. antenna count, not physical size.
- Spatial diversity → **high throughput**.

E. Björnson, E. G. Larsson, and T. L. Marzetta, "Massive MIMO: Ten Myths and One Critical Question," *IEEE Communications Magazine*, vol. 54, no. 2, pp. 114–123, 2016

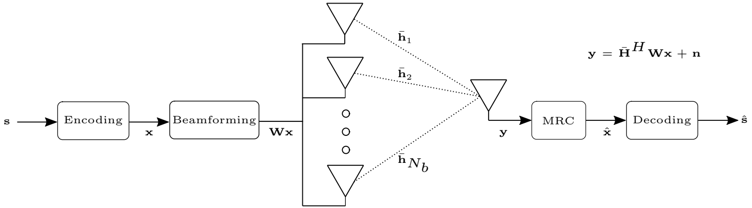

Figure: Multi-antenna transmitter (BS, gNB) and single-antenna user equipment (UE) with relevant system values.

In OFDM, the fading coefficients between Tx/Rx = **Channel State Information (CSI)**, $\bar{\mathbf{H}}$.

$$\bar{\mathbf{H}} = \begin{bmatrix} h_{1,1} & h_{1,2} & \dots & h_{1,N_f} \\ h_{2,1} & h_{2,2} & \dots & h_{2,N_f} \\ \vdots & \vdots & \vdots & \vdots \\ h_{N_b,1} & h_{N_b,2} & \dots & h_{N_b,N_f} \end{bmatrix} \in \mathbb{C}^{N_b \times N_f}$$

For N_b transmit antennas and N_f subcarriers.

Downlink-uplink reciprocity in TDD, but not in FDD.

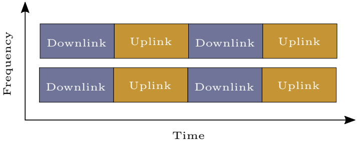

a) Time division duplex (TDD)

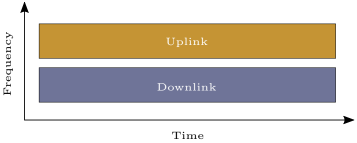

b) Frequency division duplex (FDD)

Downlink-uplink reciprocity in TDD, but not in FDD.

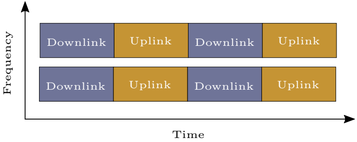

a) Time division duplex (TDD)

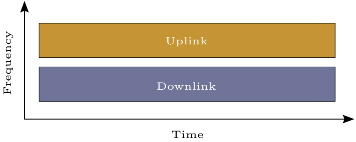

b) Frequency division duplex (FDD)

FDD requires feedback for downlink CSI estimation.

Transmitting $\bar{\mathbf{H}}$ is costly. Instead, generate estimates, $\hat{\bar{\mathbf{H}}}$, based on **compressed feedback**, $\mathbf{z}$.

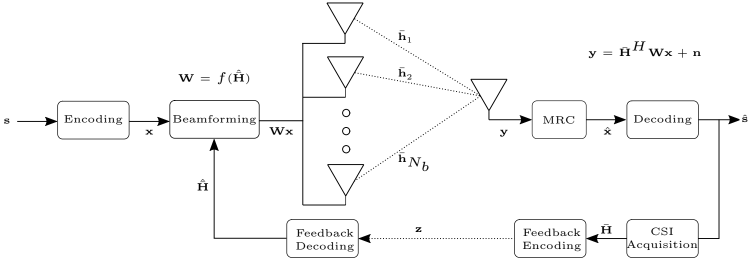

Denote 2D inverse FFT of $\bar{\mathbf{H}}$ as

$$\tilde{\mathbf{H}} = \mathbf{F}^H \bar{\mathbf{H}} \mathbf{F}.$$

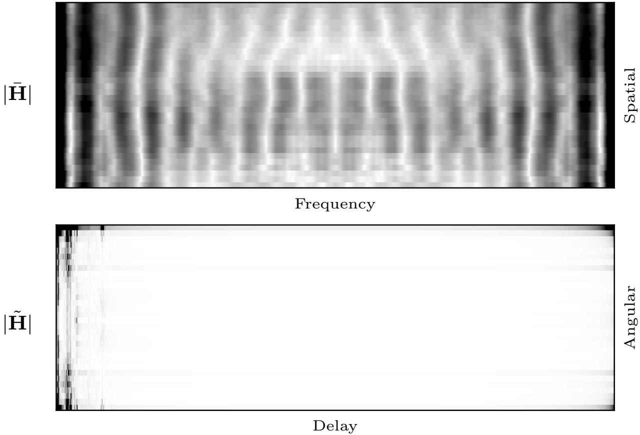

Given sparsity of $\tilde{\mathbf{H}}$, we can encode/decode a truncated version, $\mathbf{H}$.

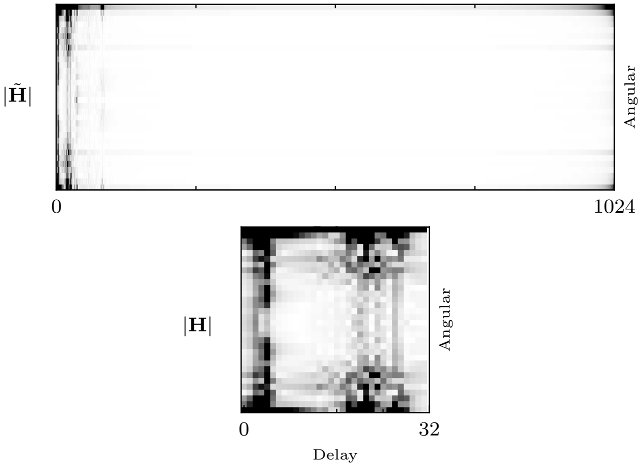

1. Compressed Sensing (Conventional)
2. Convolutional Neural Networks (This thesis)

Find low-dimensional basis for sparse data, $\mathbf{h}$,

$$\mathbf{y} = \mathbf{A}\mathbf{h} + \mathbf{n}.$$

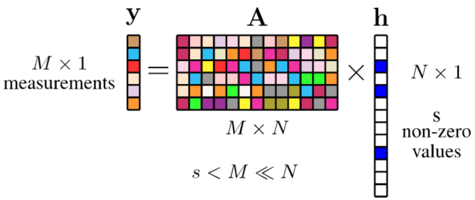

E. Crespo Marques, N. Maciel, L. Naviner, H. Cai, and J. Yang, "A Review of Sparse Recovery Algorithms," *IEEE Access*, vol. 7, pp. 1300–1322, 2019

CS addresses two major issues:

1. Design of $\mathbf{A}$ (stochastic or deterministic).

CS addresses two major issues:

1. Design of $\mathbf{A}$ (stochastic or deterministic).
2. Recovery of $\hat{\mathbf{h}}$ given $\mathbf{A}$ and $\mathbf{y}$, typically via convex optimization on p-norm minimization,

$$\min \|\hat{\mathbf{h}}\|_p \text{ subject to } \|\mathbf{y} - \mathbf{A}\hat{\mathbf{h}}\|_2^2 < \epsilon.$$

where usually $p = 1$.

CS addresses two major issues:

1. Design of $\mathbf{A}$ (stochastic or deterministic).
2. Recovery of $\hat{\mathbf{h}}$ given $\mathbf{A}$ and $\mathbf{y}$, typically via convex optimization on p-norm minimization,

$$\min \|\hat{\mathbf{h}}\|_p \text{ subject to } \|\mathbf{y} - \mathbf{A}\hat{\mathbf{h}}\|_2^2 < \epsilon.$$

where usually $p = 1$.
Problems:

- Recovery algorithms are iterative.

CS addresses two major issues:

1. Design of $\mathbf{A}$ (stochastic or deterministic).
2. Recovery of $\hat{\mathbf{h}}$ given $\mathbf{A}$ and $\mathbf{y}$, typically via convex optimization on p-norm minimization,

$$\min \|\hat{\mathbf{h}}\|_p \text{ subject to } \|\mathbf{y} - \mathbf{A}\hat{\mathbf{h}}\|_2^2 < \epsilon.$$

where usually $p = 1$.
Problems:

- Recovery algorithms are iterative.
- Complexity scales with sparsity ($M \propto s$).

- Layers of trainable linear functions followed by nonlinear 'activation' functions.
- State-of-the art performance in image processing

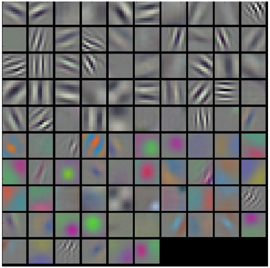

A. Karpathy, "Visualizing What ConvNets Learn," `http://cs231n.github.io/understanding-cnn/`. Accessed: Feb 24, 2020.

- Layers of trainable linear functions followed by nonlinear ‘activation’ functions.
- State-of-the art performance in image processing

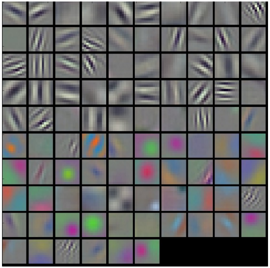

- Instantaneous decoding (non-iterative).

A. Karpathy, “Visualizing What ConvNets Learn," http://cs231n.github.io/understanding-cnn/. Accessed: Feb 24, 2020.

Autoencoder: Estimate $\hat{\mathbf{H}}$, latent code $\mathbf{Z}$ with **compression ratio**,

$$\mathrm{CR} = \frac{\dim(\mathbf{Z})}{\dim(\mathbf{H})} \text{ s.t. } \dim(\mathbf{Z}) < \dim(\mathbf{H}).$$

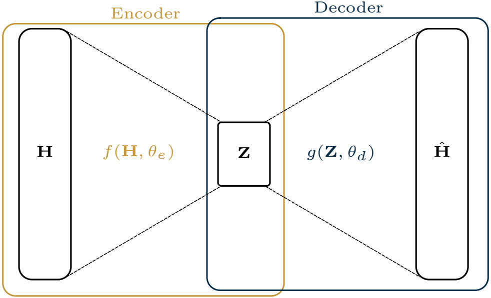

CNN Autoencoder

Autoencoder: Estimate $\hat{\mathbf{H}}$, latent code $\mathbf{Z}$ with **compression ratio**,

$$\mathrm{CR} = \frac{\dim(\mathbf{Z})}{\dim(\mathbf{H})} \text{ s.t. } \dim(\mathbf{Z}) < \dim(\mathbf{H}).$$

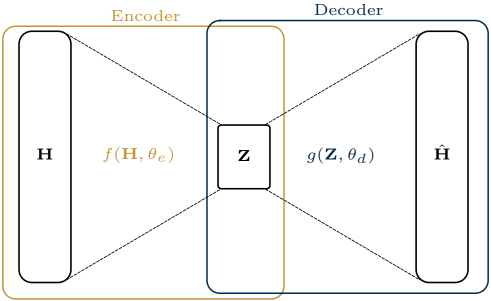

θ_e, θ_d updated to minimize **mean-squared error (MSE)**,

$$\underset{\theta_e, \theta_d}{\operatorname{argmin}} \frac{1}{N} \sum_{i=1}^{N} \|\mathbf{H}_i - g(f(\mathbf{H}_i, \theta_e), \theta_d)\|^2.$$

- CNN autoencoder for learned CSI compression and feedback [3]

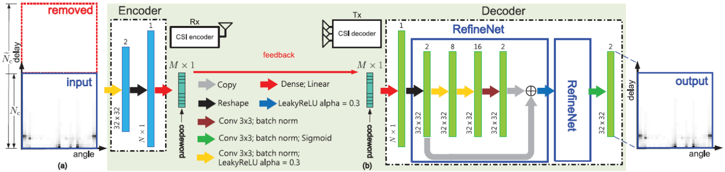

C. Wen, W. Shih, and S. Jin, "Deep Learning for Massive MIMO CSI Feedback," *IEEE Wireless Communications Letters*, vol. 7, pp. 748–751, Oct 2018

CNNs outperform CS at comparable compression ratios.

γ	Methods	Indoor		Outdoor	
		NMSE	ρ	NMSE	ρ
1/4	LASSO	-7.59	0.91	-5.08	0.82
	BM3D-AMP	-4.33	0.80	-1.33	0.52
	TVAL3	-14.87	0.97	-6.90	0.88
	CS-CsiNet	-11.82	0.96	-6.69	0.87
	CsiNet	**-17.36**	**0.99**	**-8.75**	**0.91**
1/16	LASSO	-2.72	0.70	-1.01	0.46
	BM3D-AMP	0.26	0.16	0.55	0.11
	TVAL3	-2.61	0.66	-0.43	0.45
	CS-CsiNet	-6.09	0.87	-2.51	0.66
	CsiNet	**-8.65**	**0.93**	**-4.51**	**0.79**
1/32	LASSO	-1.03	0.48	-0.24	0.27
	BM3D-AMP	24.72	0.04	22.66	0.04
	TVAL3	-0.27	0.33	0.46	0.28
	CS-CsiNet	-4.67	0.83	-0.52	0.37
	CsiNet	**-6.24**	**0.89**	**-2.81**	**0.67**
1/64	LASSO	-0.14	0.22	-0.06	0.12
	BM3D-AMP	0.22	0.04	25.45	0.03
	TVAL3	0.63	0.11	0.76	0.19
	CS-CsiNet	-2.46	0.68	-0.22	0.28
	CsiNet	**-5.84**	**0.87**	**-1.93**	**0.59**

C. Wen, W. Shih, and S. Jin, "Deep Learning for Massive MIMO CSI Feedback," *IEEE Wireless Communications Letters*, vol. 7, pp. 748–751, Oct 2018

CsiNet vs. Compressed Sensing

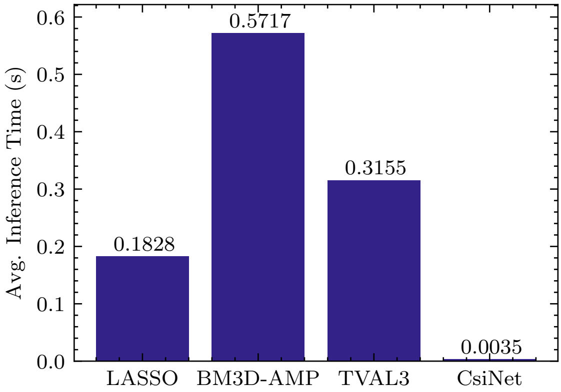

Figure: Average inference time for compressed sensing methods vs. CsiNet.

C. Wen, W. Shih, and S. Jin, "Deep Learning for Massive MIMO CSI Feedback," *IEEE Wireless Communications Letters*, vol. 7, pp. 748–751, Oct 2018

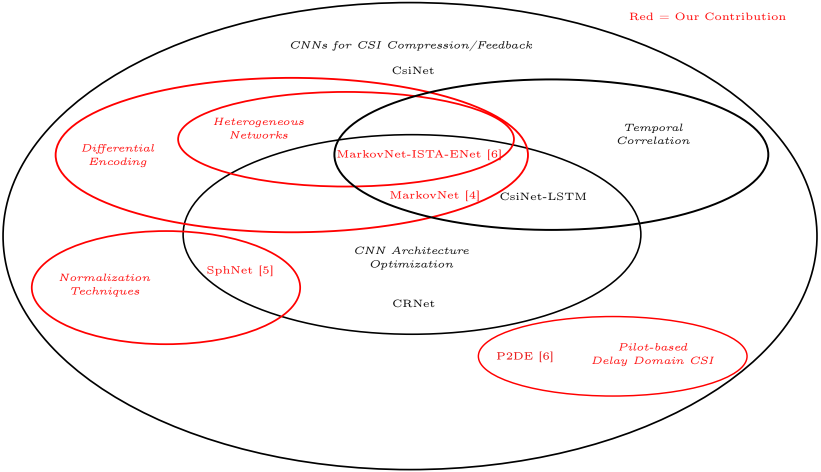

Figure: Areas of *domain knowledge* and corresponding CNNs.

Completed Work #1: SphNet

Power-based normalization for improved CSI reconstruction accuracy.

CSI vs. Images: Channels

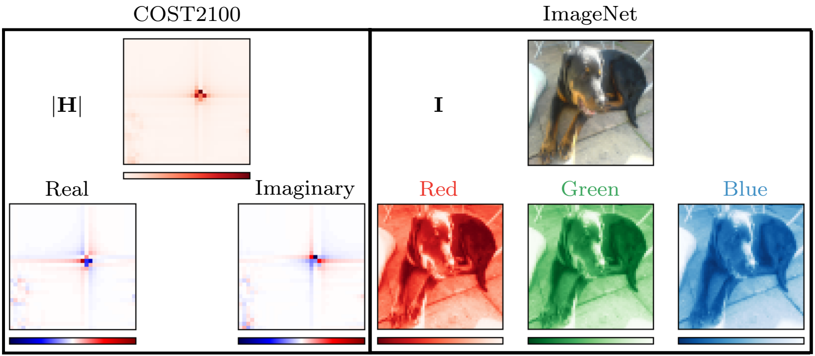

CSI vs. Images: CNNs

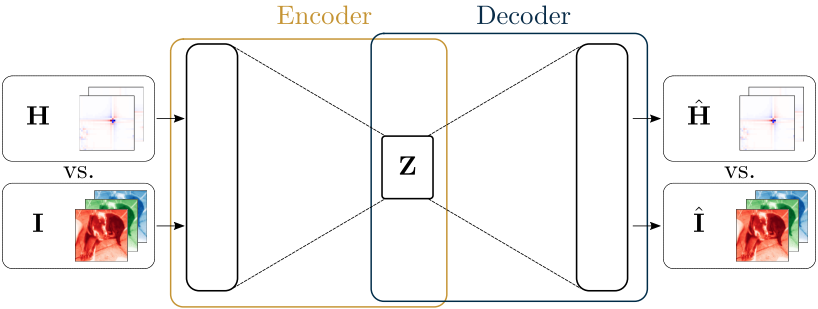

- **Minmax normalization** – Find minimum, maximum of channels.

- **Minmax normalization** – Find minimum, maximum of channels.
- $H_{n,(i,j)} = (i,j)$-th element of n-th sample

$$H_{\text{minmax},n,(i,j)} = \frac{H_{n,(i,j)} - H_{\text{min}}}{H_{\text{max}} - H_{\text{min}}} \in [0,1]$$

- **Minmax normalization** – Find minimum, maximum of channels.
- $H_{n,(i,j)} = (i,j)$-th element of n-th sample

$$H_{\mathrm{minmax},n,(i,j)} = \frac{H_{n,(i,j)} - H_{\min}}{H_{\max} - H_{\min}} \in [0,1]$$

- Compatible with common **activation functions** (e.g., tanh, sigmoid)

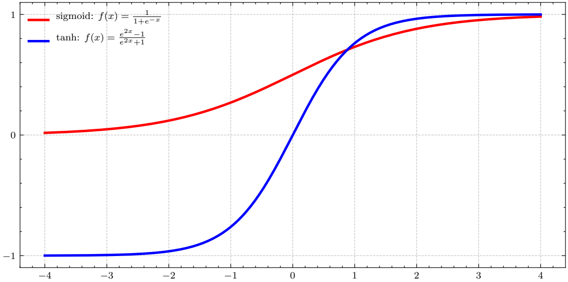

Difference of **four orders of magnitude**.

Dataset	**Env**	**Channels**	**Norm**	**Avg. Variance**
ImageNet	-	RGB	Minmax	$\underline{7.09E^{-2}}$
COST2100	Indoor	Real, Imag	Minmax	$\underline{9.98E^{-6}}$
COST2100	Outdoor	Real, Imag	Minmax	$\underline{4.02E^{-6}}$

Table: Minmax normalization applied to COST2100 and ImageNet dataset.

Spherical normalization – scale $\mathbf{H}$ by power. For Frobenius norm $\|\cdot\|$,

$$\check{\mathbf{H}}^n = \frac{\mathbf{H}^n}{\|\mathbf{H}^n\|}. \tag{1}$$

Then apply minmax scaling to the entire dataset.

Difference is now **two orders of magnitude**.

Dataset	**Env**	**Channels**	**Norm**	**Avg. Variance**
ImageNet	-	RGB	Minmax	$\underline{7.09E^{-2}}$
COST2100	Indoor	Real, Imag	Spherical	$\underline{1.41E^{-4}}$
COST2100	Outdoor	Real, Imag	Spherical	$\underline{1.43E^{-4}}$
COST2100	Indoor	Real, Imag	Minmax	$9.98E^{-6}$
COST2100	Outdoor	Real, Imag	Minmax	$4.02E^{-6}$

Table: Minmax vs. spherical normalization applied to COST2100 datasets compared with ImageNet.

SphNet Architecture

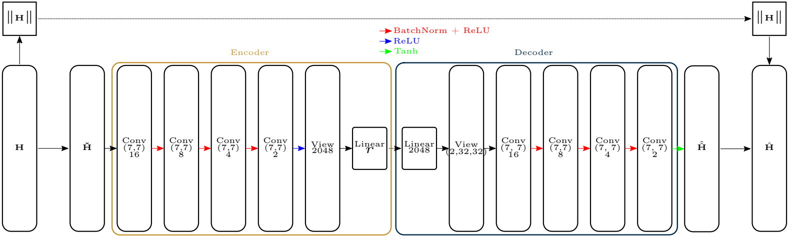

Figure: SphNet – CsiNetPro architecture with Spherical Normalization.

Z. Liu, **M. del Rosario**, X. Liang, L. Zhang, and Z. Ding, "Spherical Normalization for Learned Compressive Feedback in Massive MIMO CSI Acquisition," in *2020 IEEE International Conference on Communications Workshops (ICC Workshops)*, pp. 1–6, 2020

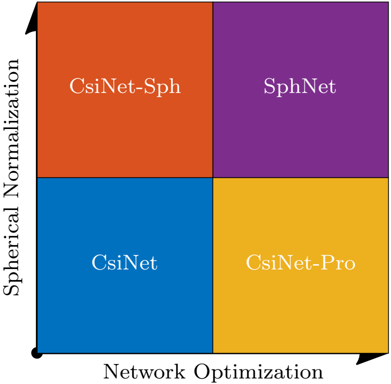

Figure: Illustration of techniques used in different models.

Z. Liu, **M. del Rosario**, X. Liang, L. Zhang, and Z. Ding, "Spherical Normalization for Learned Compressive Feedback in Massive MIMO CSI Acquisition," in *2020 IEEE International Conference on Communications Workshops (ICC Workshops)*, pp. 1–6, 2020

Table: Parameters for COST2100 model in this work.

Environment	**Indoor**	**Outdoor**
Num. BS Antennas (N_b)	32	
Num. Subcarriers (N_f)	1024	
Truncation Value (R_d)	32	
Carrier Frequency	5.3 GHz	300 MHz
UE Mobility	0.001 m/s	1 m/s
UE Starting Position	20×20 m	400×400 m
Num. Channel Samples (N)	10^5	
Training/Validation Split	70%/30%	
Feedback interval	40 ms	

L. Liu, C. Oestges, J. Poutanen, K. Haneda, P. Vainikainen, F. Quitin, F. Tufvesson, and P. D. Doncker, "The COST 2100 MIMO Channel Model," *IEEE Wireless Communications*, vol. 19, pp. 92–99, December 2012

Experimental Results

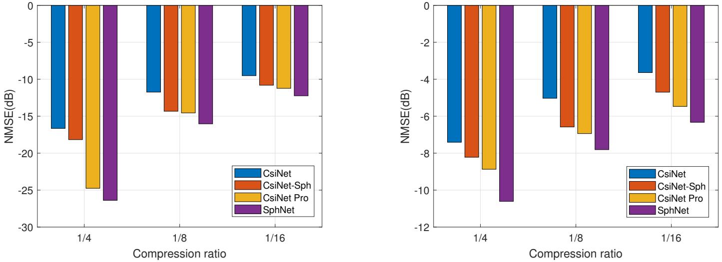

(a) Indoor (b) Outdoor

Figure: Sensitivity study for CsiNet-Pro and spherical normalization [5] (lower NMSE is better).

Z. Liu, **M. del Rosario**, X. Liang, L. Zhang, and Z. Ding, "Spherical Normalization for Learned Compressive Feedback in Massive MIMO CSI Acquisition," in *2020 IEEE International Conference on Communications Workshops (ICC Workshops)*, pp. 1–6, 2020

Completed Work #2: MarkovNet

A deep differential autoencoder for efficient temporal learning.

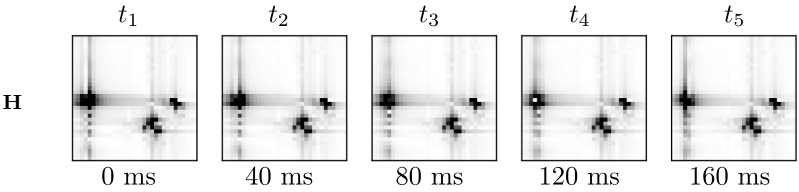

Figure: Ground truth CSI ($\mathbf{H}$) for five timeslots (T_1 through T_5) on one outdoor sample from the validation set.

Recurrent neural networks (RNNs) contain trainable long short-term memory (LSTM) cells which learn temporal relationships.

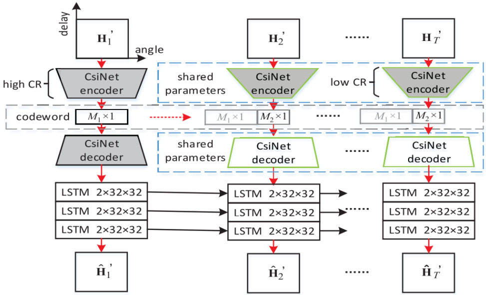

Figure: CsiNet-LSTM network architecture [8].

T. Wang, C. Wen, S. Jin, and G. Y. Li, "Deep Learning-Based CSI Feedback Approach for Time-Varying Massive MIMO Channels," *IEEE Wireless Comm. Letters*, vol. 8, pp. 416–419, April 2019

CsiNet-LSTM Performance

LSTMs improve NMSE at smaller compression ratios.

		CR	LASSO	BM3D-AMP	TVAL3	CsiNet	CsiNet-LSTM
Indoor	NMSE	1/16	-2.96	0.25	-3.20	-10.59	**-23.06**
		1/32	-1.18	20.85	-0.46	-7.35	**-22.33**
		1/64	-0.18	26.66	0.60	-6.09	**-21.24**
	ρ	1/16	0.72	0.29	0.73	0.95	**0.99**
		1/32	0.53	0.17	0.45	0.90	**0.99**
		1/64	0.30	0.16	0.24	0.87	**0.99**
	runtime	1/16	0.2471	0.3454	0.3148	**0.0001**	0.0003
		1/32	0.2137	0.5556	0.3148	**0.0001**	0.0003
		1/64	0.2479	0.6047	0.2860	**0.0001**	0.0003
	NMSE↓	1/16-1/64	94%	105	1.19	42%	**8%**
Outdoor	NMSE	1/16	-1.09	0.40	-0.53	-3.60	**-9.86**
		1/32	-0.27	18.99	0.42	-2.14	**-9.18**
		1/64	-0.06	24.42	0.74	-1.65	**-8.83**
	ρ	1/16	0.49	0.23	0.46	0.75	**0.95**
		1/32	0.32	0.16	0.28	0.63	**0.94**
		1/64	0.19	0.16	0.19	0.58	**0.93**
	runtime	1/16	0.2122	0.4210	0.3145	**0.0001**	0.0003
		1/32	0.2409	0.6031	0.2985	**0.0001**	0.0003
		1/64	0.0166	0.5980	0.2850	**0.0001**	0.0003
	NMSE↓	1/16-1/64	94%	60	2.40	54%	**10%**

T. Wang, C. Wen, S. Jin, and G. Y. Li, "Deep Learning-Based CSI Feedback Approach for Time-Varying Massive MIMO Channels," *IEEE Wireless Comm. Letters*, vol. 8, pp. 416–419, April 2019

Problem: Number of parameters/FLOPs for RNNs is large.

Table: Model size/computational complexity per timeslot for CsiNet-LSTM and CsiNet. M: million.

	Parameters		**FLOPs**	
CR	**CsiNet-LSTM**	**CsiNet**	**CsiNet-LSTM**	**CsiNet**
1/4	132.7 M	2.1 M	412.9 M	7.8 M
1/8	123.2 M	1.1 M	410.8 M	5.7 M
1/16	118.5 M	0.5 M	409.8 M	4.7 M
1/32	116.1 M	0.3 M	409.2 M	4.1 M
1/64	115.0 M	0.1 M	409.0 M	3.9 M

For short enough feedback interval, CSI data form a Markov chain,

$$\mathbf{H}_t = \gamma \mathbf{H}_{t-1} + \mathbf{V}_t,$$

with $\gamma \in \mathbb{R}^+$ and i.i.d $\mathbf{V}_t \sim \mathcal{CN}(\mathbf{0}, \Sigma_V)$.

Z. Liu †, **M. del Rosario †**, and Z. Ding, "A Markovian Model-Driven Deep Learning Framework for Massive MIMO CSI Feedback," *IEEE Transactions on Wireless Communications*, vol. 21, no. 2, pp. 1214–1228, 2022 († equal contribution)

The ordinary least-squares solution, γ, is given as

$$\gamma = \frac{\mathrm{Trace}(\mathbb{E}\left[\mathbf{H}_{t-1}^{H}\mathbf{H}_{t}\right])}{\mathbb{E}\|\mathbf{H}_{t}^{H}\mathbf{H}_{t}\|^{2}}.$$

The ordinary least-squares solution, γ, is given as

$$\gamma = \frac{\mathrm{Trace}(\mathbb{E}\left[\mathbf{H}_{t-1}^{H}\mathbf{H}_t\right])}{\mathbb{E}\|\mathbf{H}_t^{H}\mathbf{H}_t\|^2}.$$

Utilize estimator, $\hat{\gamma}$, based on the sample statistics,

$$\hat{\gamma} = \frac{\sum_{i=1}^{N} \mathrm{Trace}(\left[\mathbf{H}_{t-1}^{H}(i)\mathbf{H}_t(i)\right])}{\sum_{i=1}^{N} \|\mathbf{H}_t^{H}(i)\mathbf{H}_t(i)\|^2},$$

for training set of size N.

Using $\hat{\gamma}$, train encoder on estimation error as

$$\begin{aligned}\mathbf{E}_t &= \mathbf{H}_t - \hat{\gamma}\hat{\mathbf{H}}_{t-1} \\ \mathbf{z}_t &= f_{e,t}(\mathbf{E}_t).\end{aligned}$$

Jointly train a decoder,

$$\begin{aligned}\hat{\mathbf{E}}_t &= f_{d,t}(\mathbf{z}_t) \\ \hat{\mathbf{H}}_t &= \hat{\mathbf{E}}_t + \hat{\gamma}\hat{\mathbf{H}}_{t-1}.\end{aligned}$$

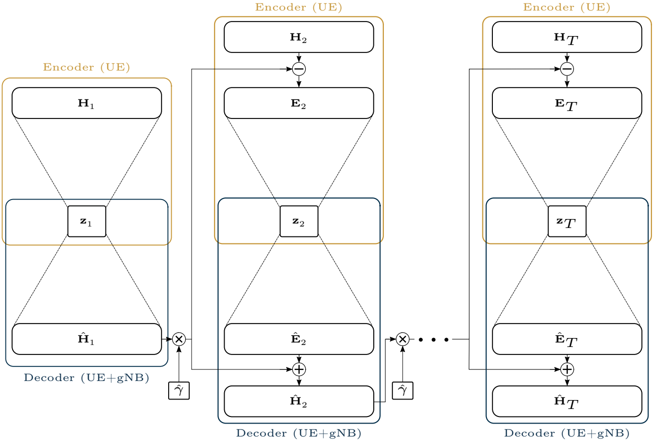

Figure: MarkovNet architecture. Networks at $t \geq 2$ predict estimation error, $\hat{\mathbf{E}}_t$.

MarkovNet Results – NMSE Performance

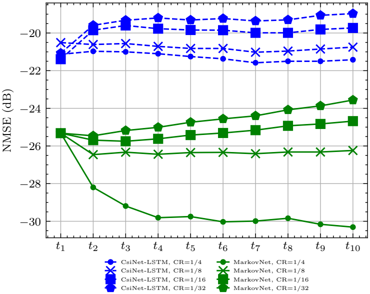

(a) Indoor

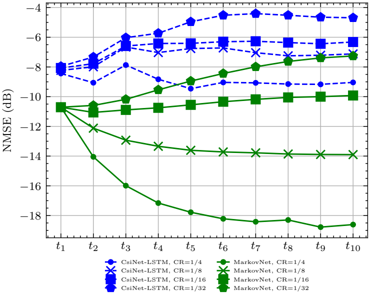

(b) Outdoor

Figure: NMSE (lower is better) comparison of MarkovNet and CsiNet-LSTM at multiple CRs.

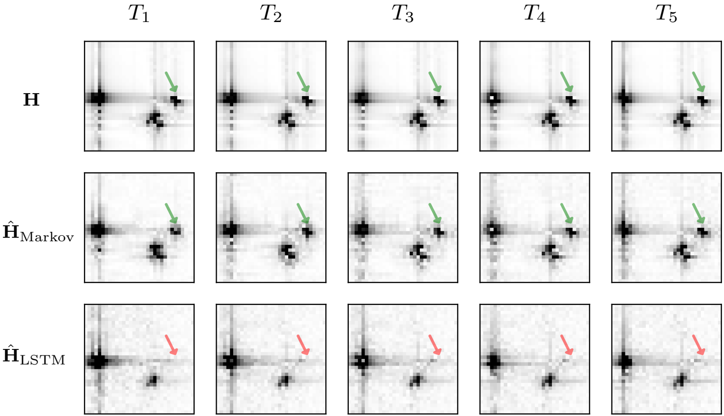

Figure: Ground truth ($\mathbf{H}$), MarkovNet estimates ($\hat{\mathbf{H}}_{\text{Markov}}$), and CsiNet-LSTM estimates ($\hat{\mathbf{H}}_{\text{LSTM}}$) on from outdoor test set ($\text{CR} = \frac{1}{4}$).

Table: Model size/computational complexity of tested temporal networks (CsiNet-LSTM, MarkovNet) and comparable non-temporal network (CsiNet). M: million.

	Parameters		
	CsiNet-LSTM	**MarkovNet**	**CsiNet**
CR=1/4	132.7 M	2.1 M	2.1 M
CR=1/8	123.2 M	1.1 M	1.1 M
CR=1/16	118.5 M	0.5 M	0.5 M
CR=1/32	116.1 M	0.3 M	0.3 M
CR=1/64	115.0 M	0.1 M	0.1 M
	FLOPs		
	CsiNet-LSTM	**MarkovNet**	**CsiNet**
CR=1/4	412.9 M	44.5 M	7.8 M
CR=1/8	410.8 M	42.4 M	5.7 M
CR=1/16	409.8 M	41.3 M	4.7 M
CR=1/32	409.2 M	40.8 M	4.1 M
CR=1/64	409.0 M	40.5 M	3.9 M

Completed Work #3: Pilots-to-delay Estimator (P2DE) and Heterogeneous Differential Encoding

Acquiring delay domain CSI under practical pilot placement. Improving differential encoding.

Recall: Works in DL-based CSI compression have used delay domain.

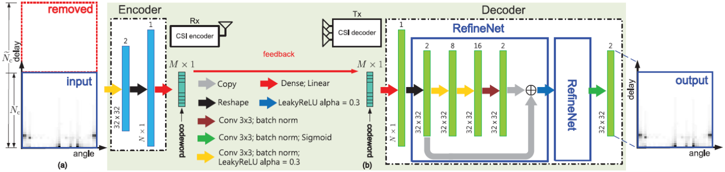

C. Wen, W. Shih, and S. Jin, "Deep Learning for Massive MIMO CSI Feedback," *IEEE Wireless Communications Letters*, vol. 7, pp. 748–751, Oct 2018

Problem: CSI at UE is based on sparse pilot estimates.

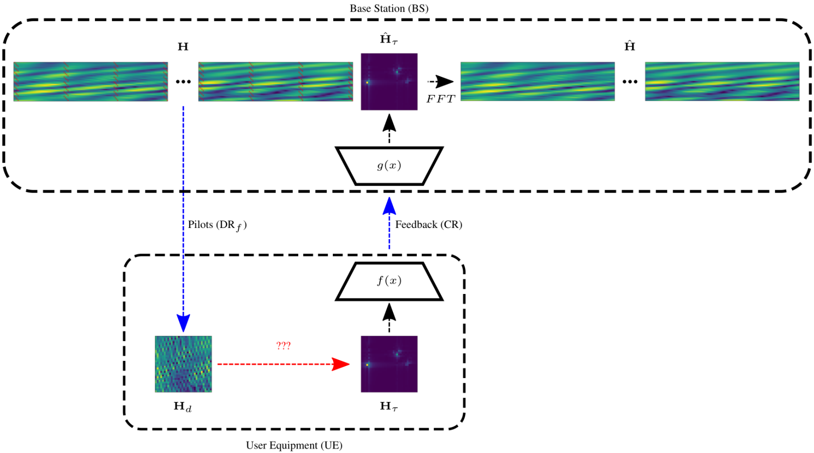

- Denote $\boldsymbol{\eta}_i \in \mathbb{C}^{N_f}$ as the i-th row of the spatial-frequency matrix $\mathbf{H}$
- Denote the downsampled version of $\boldsymbol{\eta}_i$ as $\boldsymbol{\eta}_{d,i} \in \mathbb{C}^{M_f}$ where $M_f << N_f$
- The spatial-frequency CSI, $\mathbf{H}$, and its downsampled counterpart, $\mathbf{H}_d$, can be written as,

$$\mathbf{H} = \begin{bmatrix} \boldsymbol{\eta}_1 \\ \boldsymbol{\eta}_2 \\ \vdots \\ \boldsymbol{\eta}_{N_b} \end{bmatrix} \in \mathbb{C}^{N_b \times N_f}, \ \mathbf{H}_d = \begin{bmatrix} \boldsymbol{\eta}_{d,1} \\ \boldsymbol{\eta}_{d,2} \\ \vdots \\ \boldsymbol{\eta}_{d,N_b} \end{bmatrix} \in \mathbb{C}^{N_b \times M_f}. \qquad (2)$$

Downsampled Frequency Domain CSI

- M_f = # downsampled subcarriers
- $\mathrm{DR}_f = \frac{M_f}{N_f}$ (frequency downsampling ratio)

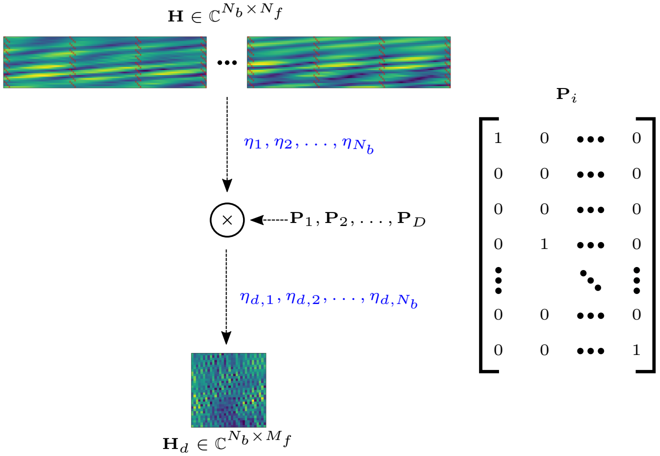

Pilot Pattern Design

- In 5G subframes, downlink pilots are allocated as **Demodulation Reference Signals (DM-RS)**.
- 'Diagonal' pilot pattern in spatial/frequency domain allows faster pilot CSI acquisition (inversely proportional to diagonal size, D)

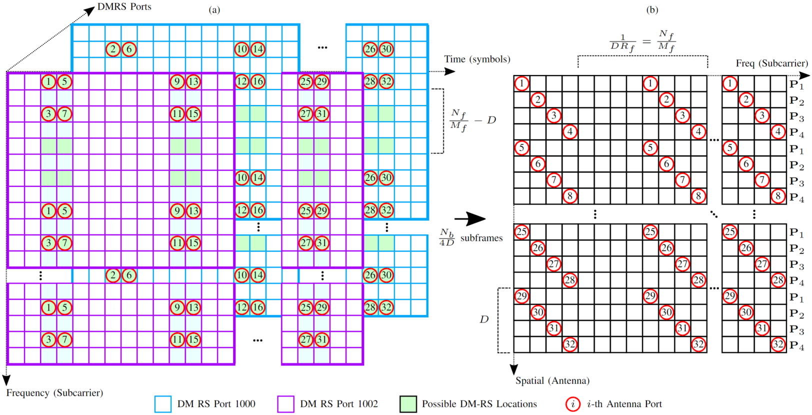

Pilots-to-Delay Estimator (P2DE)

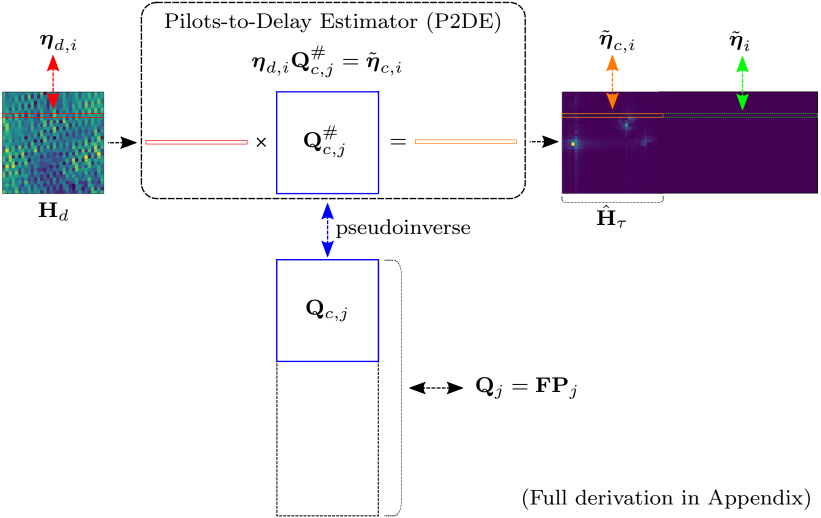

(Full derivation in Appendix)

Algorithm 1 outlines the process for acquiring truncated delay domain from sparse/downsampled frequency domain pilots.

Algorithm 1 Pilots-to-delay Estimator (P2DE) for Diagonal Pilot Pattern

Input: P2DE Matrices, $\mathbf{Q}_{c,j}^{\#}$, $j \in \{1, \ldots, D\}$
Input: Pilot spatial-frequency CSI, $\mathbf{H}_d \in \mathbb{C}^{N_b \times M_f}$
Initialize: Spatial-delay CSI, $\tilde{\mathbf{H}}_\tau \in \mathbb{C}^{N_b \times N_t}$
Initialize: Angular-delay CSI estimate, $\mathbf{H}_\tau \in \mathbb{C}^{N_b \times N_t}$
for $i = 1, 2, \ldots, N_b$ **do**
    # ***Index for*** j***-th pilot matrix***
    $j = ((i-1) \bmod D) + 1$
    # ***Apply P2D to*** i***-th antenna port***
    $\boldsymbol{\eta}_{d,i} = \mathbf{H}_d(i,:)$
    $\tilde{\mathbf{H}}_\tau(i,:) = \boldsymbol{\eta}_{d,i}\mathbf{Q}_{c,j}^{\#}$
end for
# ***Convert from spatial to angular***
$\mathbf{H}_\tau = \mathbf{F}_{N_b}\tilde{\mathbf{H}}_\tau$
Return $\mathbf{H}_\tau$

Pilots-to-Delay Estimator (P2DE)

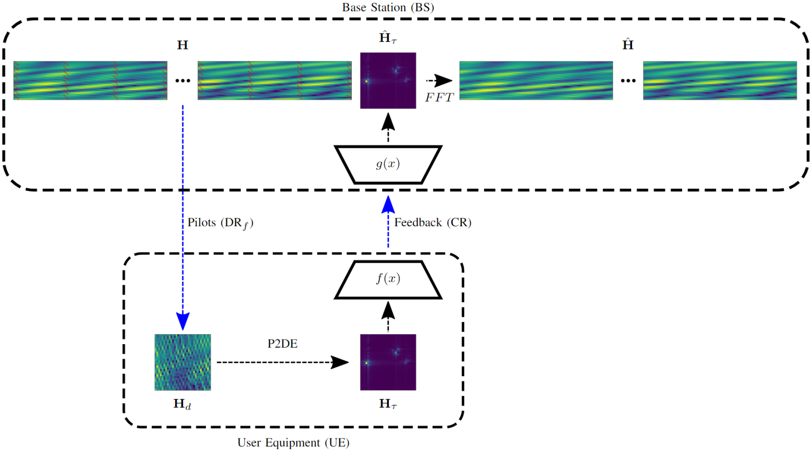

Accuracy of the P2DE at the UE (i.e., before compression and feedback) for different DR_f.

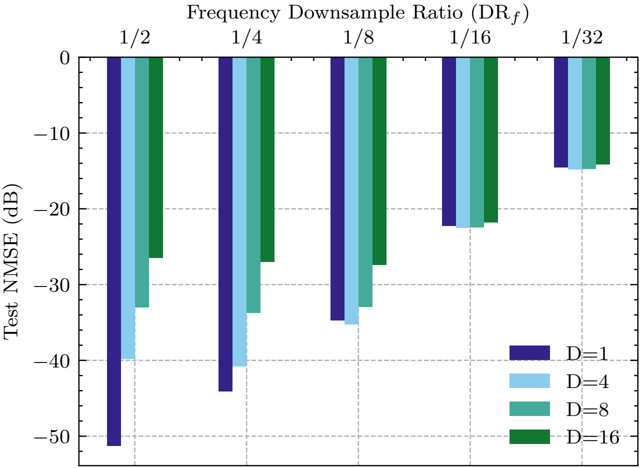

Differential encoding network using P2DE at the UE.

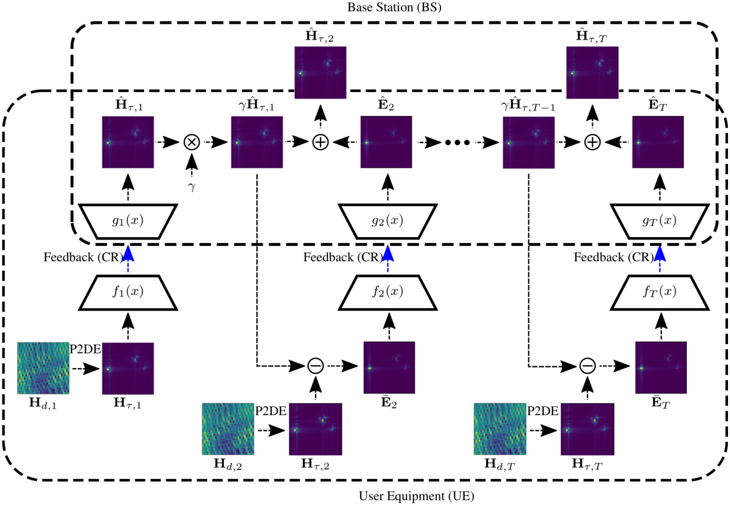

Heterogeneous Differential Encoding

- **Homogeneous:** MarkovNet used the same network at each timeslot (CsiNet Pro).
- **Heterogeneous:** Use different networks at different timeslots.

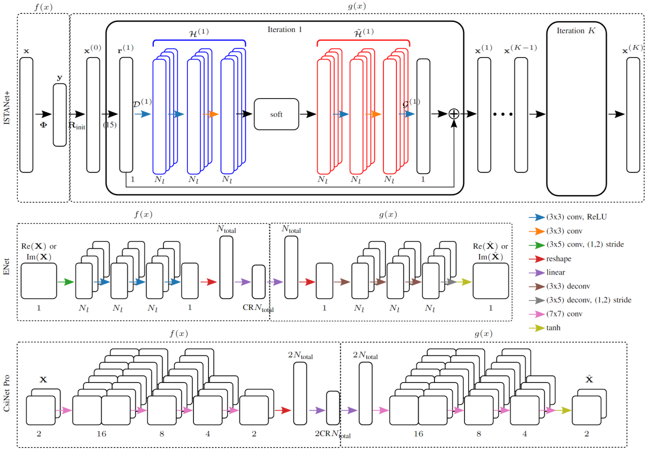

- Single timeslot performance of networks.
- Deep CS network (ISTANet+) can outperform autoencoder approaches (ENet, CsiNet Pro)
- ENet can outperform CsiNet Pro

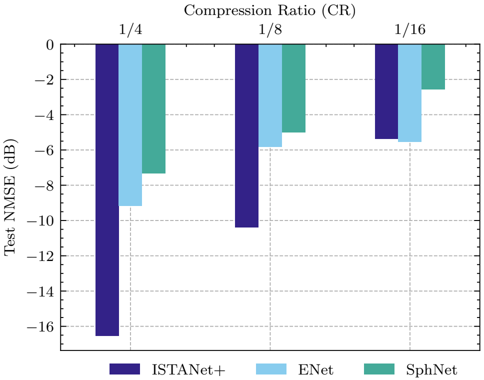

Figure: Performance comparison for different feedback compression networks using P2D estimates ($\mathrm{DF}_f = 1/16, D = 4$) for Outdoor COST2100 dataset.

Three different configurations:

- **MarkovNet-ISTA (MN-I):** *Homogeneous* MarkovNet using ISTANet+ at all timeslots $(t_1, t_2, \ldots, t_T)$.
- **MarkovNet-ENet (MN-E):** *Homogeneous* MarkovNet using ISTANet+ at all timeslots $(t_1, t_2, \ldots, t_T)$.
- **MarkovNet-ISTA-ENet (MN-IE):** *Heterogeneous* MarkovNet using ISTANet+ at t_1 and ENet at all other timeslots $(t_2, t_3, \ldots, t_T)$.

- **MN-ISTANet+**: Better performance in first timeslot.
- **MN-ENet**: Better performance in error timeslots.
- **MN-IE**: Enjoys both of the above benefits.

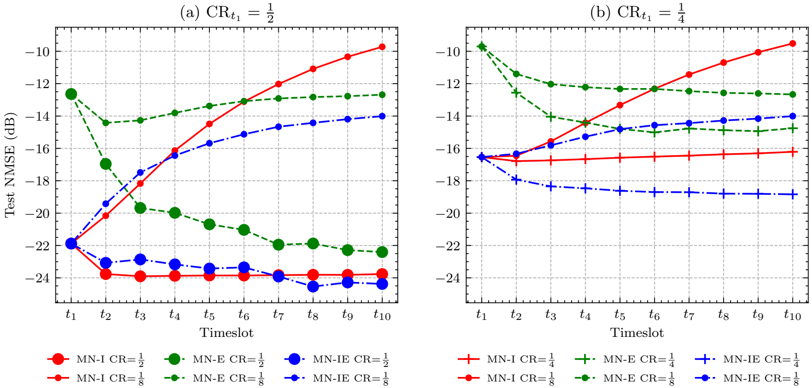

Figure: Differential encoding networks with linear P2DE as input ($M_f = 128, \mathrm{DR}_f = \frac{1}{8}, D = 4$).

Table: Computational complexity of networks used in this work (lower is better). **Bold face** in a column indicates lowest value for given compression ratio.

		Parameters (M)				FLOPs (M)	
		Trainable		All			
	CR	Enc	Dec	Enc	Dec	Enc	Dec
ISTANet+	1/2	**0.00**	**0.34**	2.10	4.54	**2.10**	393.78
	1/4	**0.00**	0.34	1.05	2.44	**1.05**	373.85
	1/8	**0.00**	0.34	0.52	1.39	**0.52**	363.89
	1/16	**0.00**	0.34	0.26	0.87	**0.26**	358.91
ENet	1/2	0.55	0.55	**0.55**	**0.55**	29.98	29.70
	1/4	0.29	**0.29**	**0.29**	**0.29**	29.46	29.18
	1/8	0.16	**0.16**	**0.16**	**0.16**	29.20	28.92
	1/16	0.09	**0.09**	**0.09**	**0.09**	29.07	28.79
CsiNet Pro	1/2	1.06	1.06	1.06	1.06	12.16	**12.16**
	1/4	0.53	0.53	0.53	0.53	11.11	**11.11**
	1/8	0.27	0.27	0.27	0.27	10.59	**10.59**
	1/16	0.14	0.14	0.14	0.14	10.33	**10.33**

- Deep CS network (ISTANet+) can provide superior initial estimate with slightly more complexity.
- Autoencoder network (ENet) can provide good error compression/estimation.
  - Fewer encoder/decoder parameters
  - More encoder FLOPs, less decoder FLOPs

Current Work: Pilot Feedback and Model Re-use

UE-focused reduction of complexity of CSI feedback.

P2DE: UE-side Computation

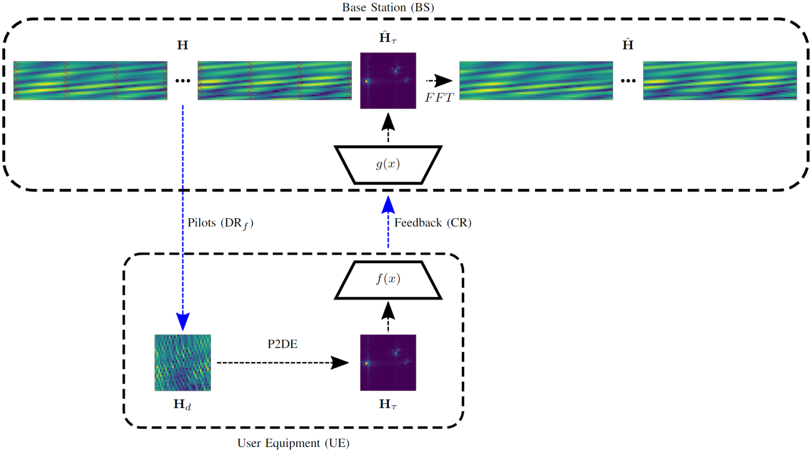

Problem: Encoder computation at (low-resourced) UE. Can we reduce this?

Table: Computational complexity of P2DE for $D = 1$ (diagonal pattern size), $N_f = 1024$ (number of subcarriers), and $N_b = 32$ (# antennas in ULA).

$\mathbf{M_f}$	**32**	**64**	**128**
FLOPs	$1.05 \cdot 10^6$	$2.10 \cdot 10^6$	$4.19 \cdot 10^6$
Parameters	$6.55 \cdot 10^4$	$1.31 \cdot 10^5$	$2.62 \cdot 10^5$

Pilot-based Feedback

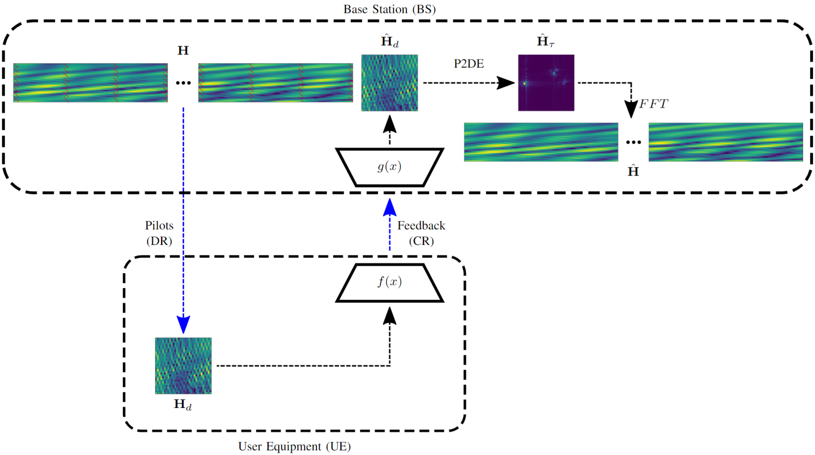

Figure: Compressive CSI estimation based on linear P2D estimator on BS side.

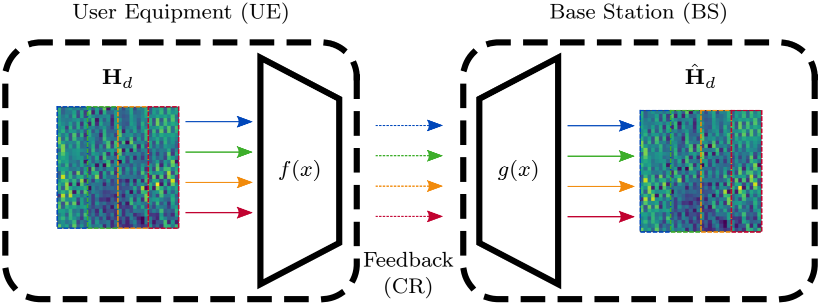

Figure: Compressive CSI estimation with model re- use. The encoder compresses K contiguous pilot subcarriers from the input, resulting in $\frac{M_f}{K}$ payloads of feedback (shown in different colors above).

Model Re-use

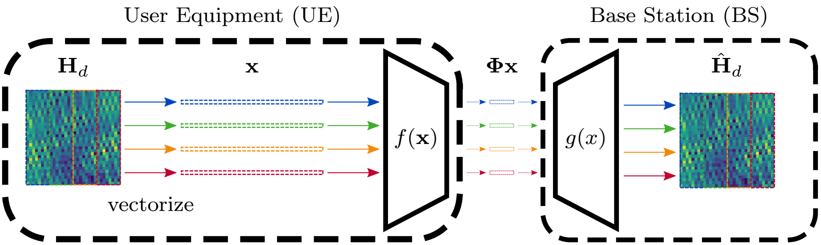

We use ISTANet+ [9], which compresses CSI at UE via,

$$f(x) = \mathbf{\Phi x} \tag{3}$$

for $\mathbf{x} \in \mathbb{R}^{N_K}$ and $\mathbf{\Phi} \in \mathbb{R}^{\mathrm{CR}N_K \times N_K}$ where $N_K = 2KN_b$

- Outdoor (top) and Indoor (bottom) results w.r.t. NMSE vs. complexity (log(FLOPs) on left, parameters on right) using different number of pilot subcarriers (M_f).
- Compare with P2DE at UE and no model re-use (red).

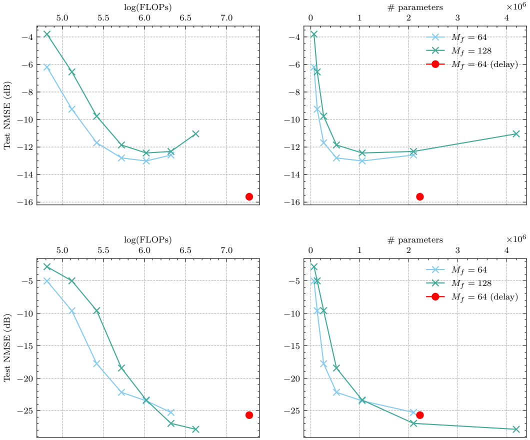

Pilot Feedback + Model Re-use: Conclusions

- Indoor: Can maintain same NMSE with 10-fold reduction in FLOPs
- Outdoor: NMSE increase of 2.5dB with 10-fold reduction in FLOPs, 10^6 reduction in parameters

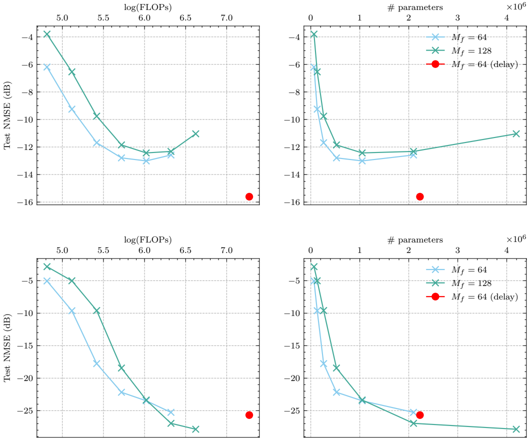

- Z. Liu, **M. del Rosario**, X. Liang, L. Zhang, and Z. Ding, “Spherical Normalization for Learned Compressive Feedback in Massive MIMO CSI Acquisition,” in *2020 IEEE International Conference on Communications Workshops (ICC Workshops)*, pp. 1–6, 2020
- Z. Liu †, **M. del Rosario †**, and Z. Ding, “A Markovian Model-Driven Deep Learning Framework for Massive MIMO CSI Feedback,” *IEEE Transactions on Wireless Communications*, vol. 21, no. 2, pp. 1214–1228, 2022
- **M. del Rosario** and Z. Ding, “Learning-Based MIMO Channel Estimation under Spectrum Efficient Pilot Allocation and Feedback,” *IEEE Transactions on Wireless Communications*, pp. 1–1, 2022
- **M. del Rosario** and Z. Ding, “Direct Pilot Feedback and Model Re-use for Encoder-focused Complexity Reduction in Massive MIMO CSI Feedback,” 2022. "In Preparation."

- Thesis committee

Acknowledgements

- Thesis committee
- Prof. Ding, lab mates, collaborators

Acknowledgements

- Thesis committee
- Prof. Ding, lab mates, collaborators
- My parents, my brother

Acknowledgements

- Thesis committee
- Prof. Ding, lab mates, collaborators
- My parents, my brother
- My SO

Questions?

`mdelrosa@ucdavis.edu`

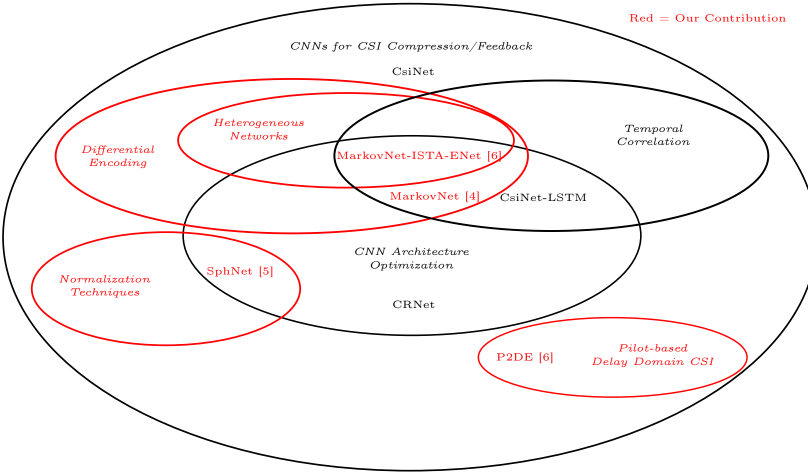

[1] E. Björnson, E. G. Larsson, and T. L. Marzetta, “Massive MIMO: Ten Myths and One Critical Question,” *IEEE Communications Magazine*, vol. 54, no. 2, pp. 114–123, 2016.

[2] E. Crespo Marques, N. Maciel, L. Naviner, H. Cai, and J. Yang, “A Review of Sparse Recovery Algorithms,” *IEEE Access*, vol. 7, pp. 1300–1322, 2019.

[3] C. Wen, W. Shih, and S. Jin, “Deep Learning for Massive MIMO CSI Feedback,” *IEEE Wireless Communications Letters*, vol. 7, pp. 748–751, Oct 2018.

[4] Z. Liu †, **M. del Rosario †**, and Z. Ding, “A Markovian Model-Driven Deep Learning Framework for Massive MIMO CSI Feedback,” *IEEE Transactions on Wireless Communications*, vol. 21, no. 2, pp. 1214–1228, 2022.

[5] Z. Liu, **M. del Rosario**, X. Liang, L. Zhang, and Z. Ding, “Spherical Normalization for Learned Compressive Feedback in Massive MIMO CSI Acquisition,” in *2020 IEEE International Conference on Communications Workshops (ICC Workshops)*, pp. 1–6, 2020.

[6] **M. del Rosario** and Z. Ding, “Learning-Based MIMO Channel Estimation under Spectrum Efficient Pilot Allocation and Feedback,” *IEEE Transactions on Wireless Communications*, pp. 1–1, 2022.

[7] L. Liu, C. Oestges, J. Poutanen, K. Haneda, P. Vainikainen, F. Quitin, F. Tufvesson, and P. D. Doncker, “The COST 2100 MIMO Channel Model,” *IEEE Wireless Communications*, vol. 19, pp. 92–99, December 2012.

[8] T. Wang, C. Wen, S. Jin, and G. Y. Li, “Deep Learning-Based CSI Feedback Approach for Time-Varying Massive MIMO Channels,” *IEEE Wireless Comm. Letters*, vol. 8, pp. 416–419, April 2019.

[9] J. Zhang and B. Ghanem, “ISTA-Net: Interpretable Optimization-inspired Deep Network for Image Compressive Sensing,” in *Proceedings of the IEEE conference on computer vision and pattern recognition*, pp. 1828–1837, 2018.

[10] **M. del Rosario** and Z. Ding, “Direct Pilot Feedback and Model Re-use for Encoder-focused Complexity Reduction in Massive MIMO CSI Feedback,” 2022.

"In Preparation.".

Note: †equal contribution

Appendix

Metrics used:

- **Normalized Mean-squared Error**

$$\mathrm{NMSE} = \frac{1}{N} \sum_{i}^{N} \frac{\|\mathbf{H}_i - \hat{\mathbf{H}}_i\|^2}{\|\mathbf{H}_i\|^2}$$

- **Cosine Similarity**

$$\rho = \frac{1}{N N_f} \sum_{i=1}^{N} \sum_{m=1}^{N_f} \frac{|\hat{\bar{\mathbf{h}}}_{i,m}^{H} \bar{\mathbf{h}}_{i,m}|}{\|\hat{\bar{\mathbf{h}}}_{i,m}\| \|\bar{\mathbf{h}}_{i,m}\|},$$

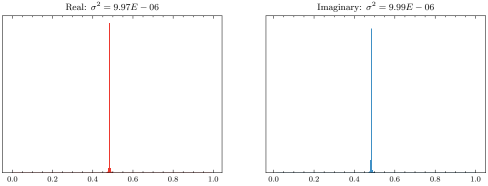

(a) Indoor

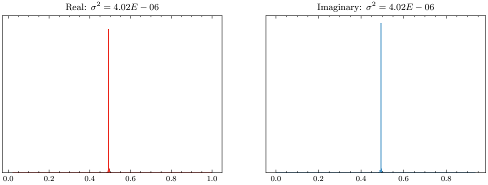

(b) Outdoor

Figure: Distribution/variance of COST2100 real/imaginary channels under minmax normalization ($N = 10^5$).

ImageNet: Minmax Normalization

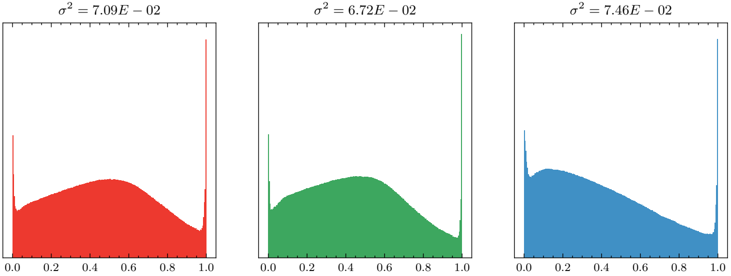

Figure: Distribution and variance of minmax-normalized ImageNet RGB channels ($N = 50000$).

COST2100: Spherical Normalization

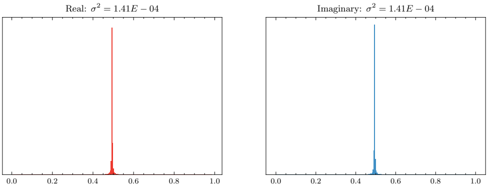

(a) Indoor

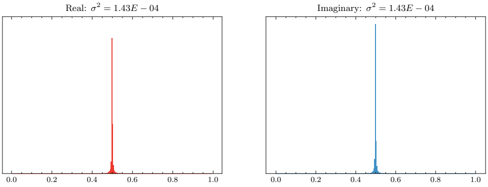

(b) Outdoor

Figure: Distribution/variance of COST2100 real/imaginary channels under spherical normalization ($N = 10^5$).

SphNet (and benchmark networks)

- **Epochs**: 1000
- **Optimizer**: Adam with learning rate 10^{-3}

MarkovNet

- **Epochs** (t_1): 1000
- **Epochs** $(t_2, \dots, t_T)$: 150
- **Optimizer**: Adam with learning rate 10^{-3}
- Each timeslot is initialized with weights from previous timeslot.

CsiNet-LSTM

- **Epochs**: 1000 (pretraining CsiNet), 500 (CsiNet-LSTM)
- **Optimizer**: Adam with learning rate 10^{-3}

D-AMP = Denoising approximate message passing. Initialize $x^0 = \mathbf{0}$, and alternate between:

$$x^{t+1} = D_{\hat{\sigma}^t}(x^t + \mathbf{A}^* z^t)$$

$$z^t = y - \mathbf{A}x^t + z^{t-1}\frac{\mathrm{div}D_{\hat{\sigma}^{t-1}}(x^{t-1} + \mathbf{A}^* z^{t-1})}{m}$$

where $\hat{\sigma}^t = \mathrm{Var}(x^t + \mathbf{A}^* z^t)$, $D_{\hat{\sigma}_t}$ = denoising algorithm.

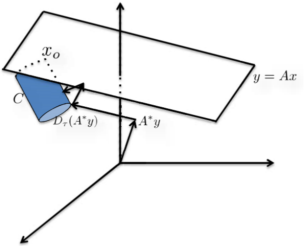

Figure: Subspaces of interest in D-AMP.

BM3D-AMP: Definition

BM3D-AMP = D-AMP with *block matching 3D collaborative filtering (BM3D)*.

- Combination of non-local means (NLM) and wavelet thresholding.
- Procedure:
  1. Compare patches of pixels in images
  2. Group similar patches
  3. 2D (DCT or Bior Wavelet) + 1D Haar wavelet transforms on group
  4. Shrink coefficients in groups ($N \to M$)
  5. Perform inverse transform by 1) hard thresholding and 2) Wiener filter ($M \to N$)

Tanh Normalization

Given mean μ, standard deviation σ w.r.t $\mathbf{H}$,

$$H_{\tanh}(i, j) = \tanh\left(\frac{H(i, j) - \mu}{2\nu\sigma}\right) + 1.$$

Scale parameter ν chosen by designer.

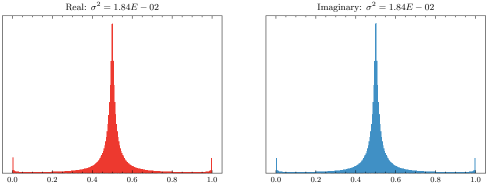

(a) $\nu = 1$

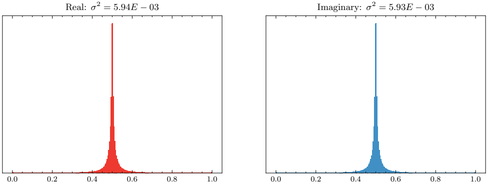

(b) $\nu = 3$

Figure: Distribution/variance of indoor COST2100 real/imaginary channels under tanh normalization ($N = 9.9\dot{1}0^5$).

COST2100 (Outdoor): Tanh Normalization

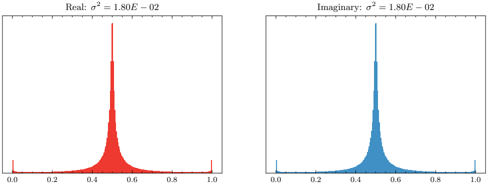

(a) $\nu = 1$

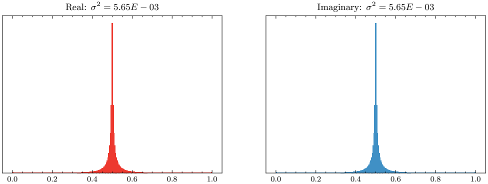

(b) $\nu = 3$

Figure: Distribution/variance of outdoor COST2100 real/imaginary channels under tanh normalization ($N = 10^5$).

MSE/NMSE equivalence

Spherical normalization $\rightarrow$ MSE equivalent to NMSE.

$$\text{MSE} = \frac{1}{N}\sum_{k=1}^{N}\|\mathbf{H}_k - \hat{\mathbf{H}}_k\|^2, \quad \text{NMSE} = \frac{1}{N}\sum_{k=1}^{N}\frac{\|\mathbf{H}_k - \hat{\mathbf{H}}_k\|^2}{\|\mathbf{H}_k\|}$$

MSE/NMSE equivalence

Spherical normalization $\to$ MSE equivalent to NMSE.

$$\mathrm{MSE} = \frac{1}{N}\sum_{k=1}^{N} \|\mathbf{H}_k - \hat{\mathbf{H}}_k\|^2, \quad \mathrm{NMSE} = \frac{1}{N}\sum_{k=1}^{N} \frac{\|\mathbf{H}_k - \hat{\mathbf{H}}_k\|^2}{\|\mathbf{H}_k\|}$$

MSE of spherically normalized estimator yields,

$$\begin{aligned}
\mathrm{MSE}_{\mathrm{Sph}} &= \frac{1}{N}\sum_{k=1}^{N} \|\check{\mathbf{H}}_k - \hat{\check{\mathbf{H}}}_k\|^2 \\
&= \frac{1}{N}\sum_{k=1}^{N} \left\| \frac{\mathbf{H}_k}{\|\mathbf{H}_k\|} - \frac{\hat{\mathbf{H}}_k}{\|\mathbf{H}_k\|} \right\|^2 \\
&= \frac{1}{N}\sum_{k=1}^{N} \frac{\|\mathbf{H}_k - \hat{\mathbf{H}}_k\|^2}{\|\mathbf{H}_k\|}.
\end{aligned}$$

Rather than scalar $\hat{\gamma} \in \mathbb{R}^+$, we can derive a multivariate p-step predictor, $\mathbf{W}_1, \ldots, \mathbf{W}_p$. Given p prior CSI samples, the mean-square optimal predictor $\hat{H}_t$ is a linear combination of these the prior CSI samples,

$$\hat{\mathbf{H}}_t = \mathbf{H}_{t-1}\mathbf{W}_1 + \cdots + \mathbf{H}_{t-p}\mathbf{W}_p + \mathbf{E}_t. \tag{4}$$

Error terms are uncorrelated with the CSI samples (i.e. $\mathbf{H}_{t-i}^H \mathbf{E}_t = 0$ for all $i \in [0, \ldots, p]$), and we pre-multiply by $\mathbf{H}_{t-i}^H$,

$$\begin{aligned} \mathbf{H}_{t-i}^H \hat{\mathbf{H}}_t &= \mathbf{H}_{t-i}^H \mathbf{H}_{t-1} \mathbf{W}_1 + \cdots + \mathbf{H}_{t-i}^H \mathbf{H}_{t-p} \mathbf{W}_p + \mathbf{H}_{t-i}^H \mathbf{E}_t \\ &= \mathbf{H}_{t-i}^H \mathbf{H}_{t-1} \mathbf{W}_1 + \cdots + \mathbf{H}_{t-i}^H \mathbf{H}_{t-p} \mathbf{W}_p. \end{aligned} \tag{5}$$

Denote the correlation matrix $\mathbf{R}_i = \mathbb{E}[\mathbf{H}_{t-i}^H \mathbf{H}_t]$. Presume CSI matrices arise from a stationary process, implying the following properties:

1. $\mathbf{R}_i = \mathbb{E}[\mathbf{H}_{t-i}^H \mathbf{H}_t] = \mathbb{E}[\mathbf{H}_t^H \mathbf{H}_{t+i}]$
2. $\mathbf{R}_i = \mathbf{R}_{-i}^H$

Taking the expectation, write (5) as a linear combination of $\mathbf{R}$,

$$\mathbf{R}_{i+1} = \mathbf{R}_i \mathbf{W}_1 + \cdots + \mathbf{R}_{i-p+1} \mathbf{W}_p.$$

For p CSI samples, write a system of p equations, admitting the following,

$$\begin{bmatrix} \mathbf{R}_1 \\ \mathbf{R}_2 \\ \dots \\ \mathbf{R}_p \end{bmatrix} = \begin{bmatrix} \mathbf{R}_0 & \mathbf{R}_1^H & \dots & \mathbf{R}_{p-1}^H \\ \mathbf{R}_1 & \mathbf{R}_0 & \dots & \mathbf{R}_{p-2}^H \\ \vdots & & \ddots & \vdots \\ \mathbf{R}_{p-1} & \mathbf{R}_{p-2} & \dots & \mathbf{R}_0 \end{bmatrix} \begin{bmatrix} \mathbf{W}_1 \\ \mathbf{W}_2 \\ \dots \\ \mathbf{W}_p \end{bmatrix}.$$

Solving for the coefficient matrices admits the solution

$$\begin{bmatrix} \mathbf{W}_1 \\ \mathbf{W}_2 \\ \dots \\ \mathbf{W}_p \end{bmatrix} = \begin{bmatrix} \mathbf{R}_0 & \mathbf{R}_1^H & \dots & \mathbf{R}_{p-1}^H \\ \mathbf{R}_1 & \mathbf{R}_0 & \dots & \mathbf{R}_{p-2}^H \\ \vdots & & \ddots & \vdots \\ \mathbf{R}_{p-1} & \mathbf{R}_{p-2} & \dots & \mathbf{R}_0 \end{bmatrix}^+ \begin{bmatrix} \mathbf{R}_1 \\ \mathbf{R}_2 \\ \dots \\ \mathbf{R}_p \end{bmatrix}, \tag{6}$$

where $[\cdot]^+$ denotes the Moore-Penrose pseudoinverse.

NMSE: All vs. Truncated

$$\mathrm{NMSE}_{\mathrm{all}} = \frac{1}{N}\sum_{i}^{N}\frac{\|\tilde{\mathbf{H}}_i - \hat{\tilde{\mathbf{H}}}_i\|^2}{\|\tilde{\mathbf{H}}_i\|^2},\ \mathrm{NMSE}_{\mathrm{truncate}} = \frac{1}{N}\sum_{i}^{N}\frac{\|\mathbf{H}_i - \hat{\mathbf{H}}_i\|^2}{\|\mathbf{H}_i\|^2},$$

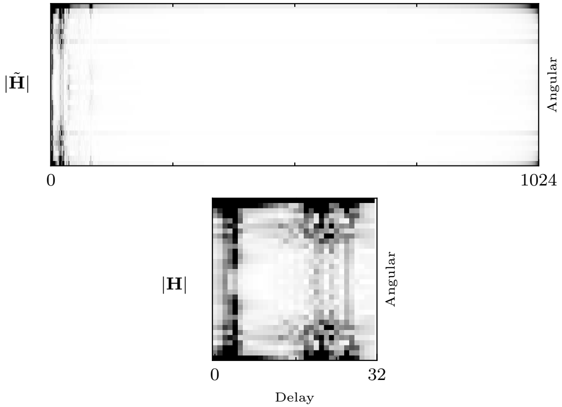

MarkovNet: All vs. Truncated

		MarkovNet		CsiNet-LSTM	
Env	**CR**	$\text{NMSE}_{\text{truncate}}$	NMSE_{all}	$\text{NMSE}_{\text{truncate}}$	NMSE_{all}
Indoor	$\frac{1}{4}$	-29.26	-20.81	-21.28	-18.4
	$\frac{1}{8}$	-26.25	-20.26	-20.76	-18.12
	$\frac{1}{16}$	-25.27	-19.99	-19.96	-17.67
	$\frac{1}{32}$	-24.62	-19.78	-19.41	-17.34
Outdoor	$\frac{1}{4}$	-16.8	-12.4	-8.89	-7.99
	$\frac{1}{8}$	-13.19	-10.86	-7.17	-6.60
	$\frac{1}{16}$	-10.45	-9.13	-6.65	-6.15
	$\frac{1}{32}$	-8.87	-7.92	-5.33	-4.99

Table: NMSE of truncated vs. full CSI matrices.

MarkovNet: Results ($\text{NMSE}_{\text{truncated}}$)

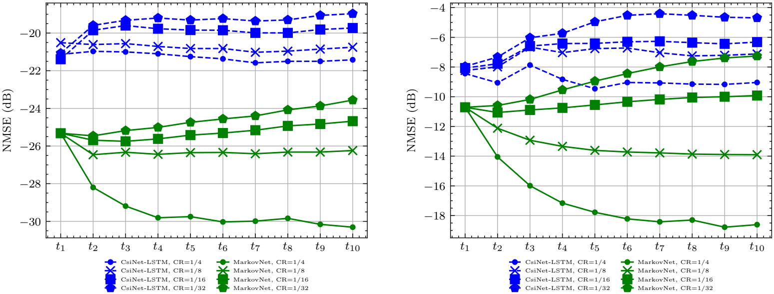

(a) Indoor (b) Outdoor

Figure: $\text{NMSE}_{\text{truncated}}$ comparison of MarkovNet and CsiNet-LSTM at various compression ratios (CR).

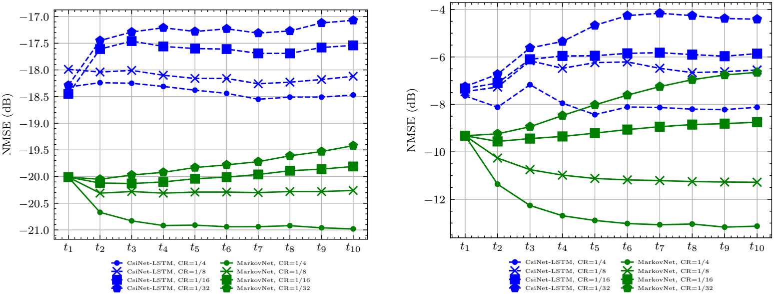

(a) Indoor (b) Outdoor

Figure: NMSE_{all} comparison of MarkovNet and CsiNet-LSTM at various compression ratios (CR).

Denote delay-domain CSI vector, $\tilde{\boldsymbol{\eta}}_i$, which is defined as

$$\tilde{\boldsymbol{\eta}}_i \mathbf{F} = \boldsymbol{\eta}_i, \tag{7}$$

for $\mathbf{F} \in \mathbf{C}^{N_f \times N_f}$ is the discrete Fourier transform (DFT) matrix.

Apply the pilot downsampling matrix $\mathbf{P}_i$ to both sides of (7),

$$\begin{aligned} \tilde{\boldsymbol{\eta}}_i \mathbf{F}\mathbf{P}_i &= \boldsymbol{\eta}_i \mathbf{P}_i \\ \tilde{\boldsymbol{\eta}}_i \mathbf{Q}_i &= \boldsymbol{\eta}_{d,i} \end{aligned} \tag{8}$$

where $\mathbf{Q}_i = \mathbf{F}\mathbf{P}_i \in \mathbb{C}^{N_f \times M_f}$ is the downsampled DFT matrix.

- **Goal:** Feed back/compress truncated delay domain vectors, $\tilde{\boldsymbol{\eta}}_{c,i} \in \mathbb{C}^{N_t}$.
- Denote zero-padded vector $\tilde{\boldsymbol{\eta}}_i$ as

$$\tilde{\boldsymbol{\eta}}_i = \left[\tilde{\boldsymbol{\eta}}_{c,i}, \mathbf{0}_{N_f - N_t}\right]. \tag{9}$$

- Based on $\mathbf{Q}_i$ of (8), the delay domain is related to the pilots by the pseudoinverse,

$$\begin{aligned} \tilde{\boldsymbol{\eta}}_i \mathbf{Q}_i \mathbf{Q}_i^T &= \boldsymbol{\eta}_{d,i} \mathbf{Q}_i^T \\ \tilde{\boldsymbol{\eta}}_i &= \boldsymbol{\eta}_{d,i} \mathbf{Q}_i^T \left(\mathbf{Q}_i \mathbf{Q}_i^T\right)^{-1} \\ &= \boldsymbol{\eta}_{d,i} \mathbf{Q}_i^{\#}. \end{aligned} \tag{10}$$

For a nearly singular matrix, stability of the matrix inverse can be improved by regularization. We use off-diagonal regularization (ODIR) to perform such regularization.

Denote A_{ij} as the i-th row and j-th column of matrix $\mathbf{A}$. Select a scaling factor $\delta \in \mathbb{R}^+$ to scale down off-diagonal elements of $\mathbf{A}$. The elements of the resulting ODIR matrix, $\mathbf{A}_{\mathrm{ODIR}}$, are written as

$$A_{ij,\mathrm{ODIR}} = \begin{cases} A_{ij} & \text{if } i = j \\ \frac{A_{ij}}{1+\delta} & \text{if } i \neq j. \end{cases} \tag{11}$$

To simulate pilot estimation error, we use additive Gaussian noise,

$$\hat{\mathbf{H}}_d = \mathbf{H}_d + \mathbf{N}_d$$

where $\mathbf{N}_d(i,j) \sim \mathcal{N}(0, \sigma^2)$ for $i \in [1, 2, \ldots, N_b]$, $j \in [1, 2, \ldots, M_f]$. We show the accuracy of the P2DE for different values of σ^2 ($D = 4, \mathrm{DR}_f = \frac{1}{32}$).

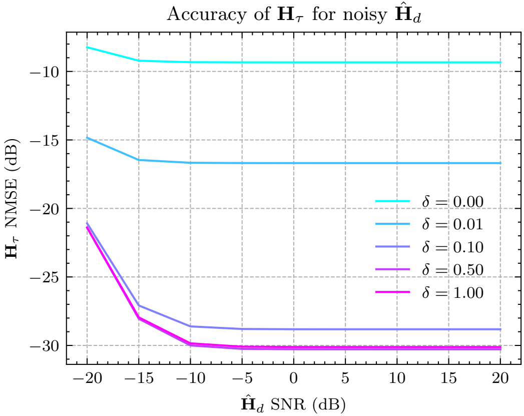

- **Iterative Shrinkage-Threshold Algorithm (ISTA)**: The solution to the proximal-gradient method for the LASSO.

$$\textbf{Gradient Step}: \mathbf{r}^{(k)} = \mathbf{x}^{(k-1)} - \rho \mathbf{\Phi}^\top (\mathbf{\Phi} \mathbf{x}^{(k-1)} - \mathbf{y}) \tag{12}$$

$$\textbf{Proximal Step}: \mathbf{x}^{(k)} = \operatorname{argmin}_{\mathbf{x}} \frac{1}{2} \|\mathbf{x} - \mathbf{r}^{(k)}\|_2^2 + \lambda \|\mathbf{\Phi} \mathbf{x}\|_1 \tag{13}$$

- Solution to proximal step = soft-threshold function,

$$\operatorname{prox}_{\lambda \|\mathbf{\Psi}\|_1}(v) = \begin{cases} v - \lambda & \text{if } \lambda < v \\ 0 & -\lambda < v < \lambda \\ v + \lambda & \text{if } v < -\lambda \end{cases}$$

$$\mathrm{prox}_{\lambda\|\boldsymbol{\Psi}\|_1}(v) = \begin{cases} v - \lambda & \text{if } \lambda < v \\ 0 & -\lambda < v < \lambda \\ v + \lambda & \text{if } v < -\lambda \end{cases}$$

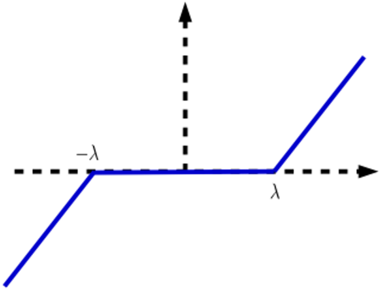

1. Need to tune hyperparameters (step size ρ, soft-threshold λ)
2. Several iterations needed to reach convergence; unreliable timing for algorithm.

- **Solution**: “Unroll” the iterations into finite, identical CNNs.
- Trainable hyperparameters (i.e., step size, threshold) per-iteration

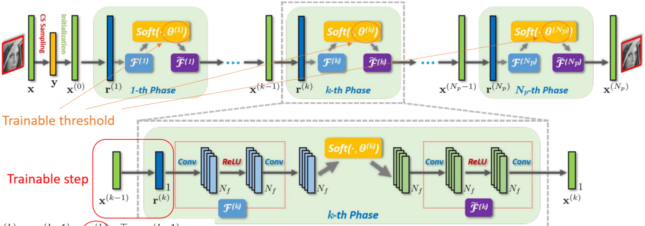

$$\mathbf{r}^{(k)} = \mathbf{x}^{(k-1)} - \rho^{(k)}\Phi^\top(\Phi\mathbf{x}^{(k-1)} - \mathbf{y}).$$